INTERNATIONAL JOURNAL FOR NUMERICAL METHODS IN FLUIDS
Int. J. Numer. Meth. Fluids 2001; **37**: 479–500 (DOI: 10.1002/fld.194)

On the shoreline boundary conditions for Boussinesq-type models

G. Bellotti[a] and M. Brocchini[b,*,1]

[a] *DITS, Università di Roma 'La Sapienza', Roma, Italy*
[b] *DIAm, Università di Genova, Genova, Italy*

SUMMARY

We propose and illustrate a novel type of shoreline boundary conditions for Boussinesq-type models. On the basis of characteristic equations of the non-linear shallow water equations, boundary conditions are developed equations that can suitably model the motion of the instantaneous shoreline. Such boundary conditions are then implemented in a numerical solver for a specific set of Boussinesq-type equations, which have been proved very effective for near-shore modelling. Finally, a number of tests are performed to validate and illustrate the behaviour of the new conditions. Copyright © 2001 John Wiley & Sons, Ltd.

KEY WORDS: Boussinesq-type models; run-up; shoreline boundary conditions

1. INTRODUCTION

The most favoured approximate model equations for studying near-shore hydrodynamics are both the classic non-linear shallow water equations (NSWEs) and the many available Boussinesq-type equations (BTEs), which all stem from the work of Peregrine [1].

BTEs became very popular when it was proved they could model fairly well breaking waves [2,3]. Subsequently, in order to make such equations more suitable for coastal engineering practice, dispersive characteristics were greatly improved extending their seaward limit to reach the so-called 'intermediate depths' (see [4] and references therein).

Notwithstanding these important improvements, which recently made BTE models 'the models' for coastal engineering, flow solvers based on those equations suffer a major problem. This is related to the mathematical/numerical treatment of both the swash motions and the delicate shoreline boundary conditions [5].

To our knowledge no available solver based on BTEs correctly models the shoreline motions and often *ad hoc* artificial techniques are used to model wave run-up and run-down (see for

* Correspondence to: Dipt. di Ingegneria Ambientale, Via Montallegro 1, 16145 Genova, Italy.
[1] E-mail: brocchinin@diam.unige.it

Received 25 May 2000
Revised 8 February 2001

example the 'slot technique' used by Madsen *et al.* [6]). The quest for good shoreline boundary conditions (SBCs) to be implemented in a BTE model is currently being pushed in a number of different directions. Recently new SBCs are being developed [7] with the use of co-ordinate transformations, which map the irregular shoreline to a straight line. Although a few examples are given that testify good performances, some doubts can be reasonably raised on the effectiveness of such techniques in the case of heavily breaking waves, which require strongly distorted transformations. This is more true for breaking waves which interact in the swash zone (e.g. backwash bores) as they generate cusp-like indentations at the shoreline which seem hardly representable by a smooth co-ordinate transformation. No artificial techniques are required when using the NSWEs as model equations. NSWEs are typically solved by means of the method of characteristics and the shoreline is a characteristic itself!

It is now becoming clear that better modelling is required of the SBCs employed in BTE models. To this purpose a number of methods can be applied, a short list of which is given here as reference.

1.1. BTE-NSWE matching

This method, currently applied by some researchers, does not directly address the real problems concerning the definition of suitable SBCs. Rather, a pragmatic view is taken according to which purely dispersive BTEs (i.e. with no extra non-linear contributions) reduce to NSWEs in very shallow waters. Consequently, a matching is imposed (depending on the local Ursell number) between BTE and NSWE solvers [8]. With this technique swash zone motions are always modelled by the NSWE module, which properly handles the motion of the shoreline.

1.2. Extension of the NSWE to include dispersion

This is based on the view that NSWEs are most suitable for modelling the swash zone motions and track the shoreline positions. In order to extend the range of validity of the NSWE to the 'intermediate depths' suitable non-linear-dispersive contributions can be included either into the flux term $\mathbf{F}_x$ or into the source term $\mathbf{S}$ of the model equations

$$\mathbf{U}_t + \mathbf{F}_x = \mathbf{S} \tag{1.1}$$

used to cast the 1DH-NSWE in a typical conservation form to be solved for the variable $\mathbf{U}$ [9].

1.3. Characteristic-type SBCs for BTEs

A third approach is here followed, which is believed to both provide a close description of what actually happens at the point (line) where the water meets the beach face and to be easily implemented in any type of numerical models based on BTEs. Analysis is underway to define the most suitable form of the SBCs for 1DH flow propagation [10]

$$\frac{\mathrm{d}x_\mathrm{s}}{\mathrm{d}t} = u_\mathrm{s}, \qquad d_\mathrm{s} = 0 \tag{1.2}$$

with x_s being the shoreline position, d_s and u_s the water depth and the flow speed at the shore respectively.

A theoretical analysis of the general technique which can be used to define SBCs for BTE models on the basis of characteristic equations is given in Section 2. Section 3 briefly illustrates the specific BTE model in which the new SBCs described in Section 4 are implemented. In Section 5 a few examples are reported which illustrate the performances of the new SBCs and their implementation. Some concluding remarks are given in the final Section 6 along with a short description of ongoing research.

2. SBCs BASED ON CHARACTERISTIC EQUATIONS

First of all it is necessary to recognize that for small enough water depth most dispersive-nonlinear terms D, which characterize BTEs from NSWEs become negligible. Hence, near the shoreline we can write the 1DH version of any BTE as

$$d_t + (ud)_x = 0 \tag{2.3a}$$

$$u_t + uu_x + gd_x = gh_x - \tau_b + D \tag{2.3b}$$

where $d = h + \zeta$ (see Figure 1) is the total water depth, u is a depth-averaged velocity, τ_b is the seabed friction and subscripts are used to represent partial derivatives.

These can be cast in suitable conservative vectorial form, which is typically used in shock-capturing numerical solvers

$$\mathbf{U}_t + \mathbf{F}(\mathbf{U})_x = \mathbf{S}(\mathbf{U}) \tag{2.4}$$

$\mathbf{U}$ being the vector of the unknowns, $\mathbf{F}$ the flux term and $\mathbf{S}$ the source term

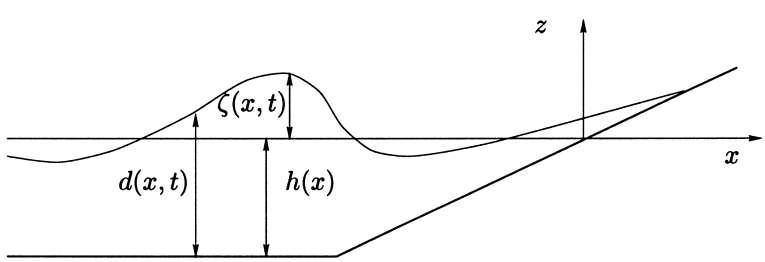

Figure 1. Sketch of typical problem geometry.

$$\mathbf{U} = \begin{bmatrix} d \\ ud \end{bmatrix}, \qquad \mathbf{F}(\mathbf{U}) = \begin{bmatrix} ud \\ u^2 d + \dfrac{gd^2}{2} \end{bmatrix}, \qquad \mathbf{S}(\mathbf{U}) = \begin{bmatrix} 0 \\ gdh_x - d\tau_b + dD \end{bmatrix} \tag{2.5}$$

which also includes all dispersive-non-linear contributions D which characterize each specific BTE.

It is useful to introduce a Riemann problem defined by Equations (2.4) and (2.5) and constant initial conditions such that

$$\mathbf{U}(x, 0) = \mathbf{U}_0(x) = \begin{cases} \mathbf{U}^{\mathrm{L}} & \text{if } x < 0 \\ \mathbf{U}^{\mathrm{R}} & \text{if } x > 0 \end{cases} \tag{2.6}$$

The Riemann problem helps to formulate and solve the transition which occurs at the shoreline from a left (constant) wet state and a right (constant) dry state (see Figure 2), a similar description was given by Stoker [11] of the 'retreating piston' or 'retreating wave paddle' problem. We call the specific Riemann problem of Figure 2(b) as the 'shoreline Riemann problem'.

Solution to this typical hyperbolic problem is given in terms of two wave families which are here called C_+ and C_- (Figure 3 represents the solution structure for the problem of Figure 2(b)). In very shallow water the characteristic curves C_- and C_+ of (2.4) are

$$\frac{\mathrm{d}x}{\mathrm{d}t} = \lambda_1 = u - c \quad (C_-), \qquad \frac{\mathrm{d}x}{\mathrm{d}t} = \lambda_2 = u + c \quad (C_+) \tag{2.7}$$

where $c = \sqrt{gd}$. These curves meet at the shoreline which can be considered as a C_--type characteristic such that

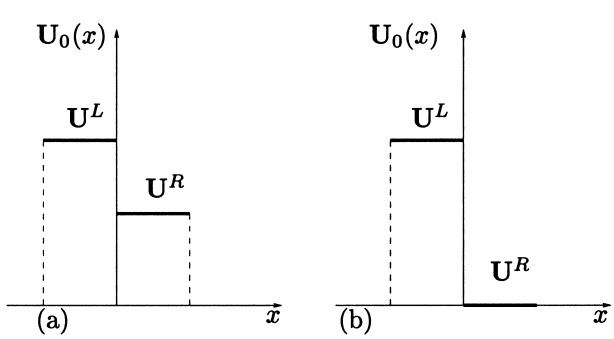

Figure 2. The Riemann problem. Illustration of the initial data for: (a) a generic Riemann problem, (b) the 'shoreline Riemann problem'.

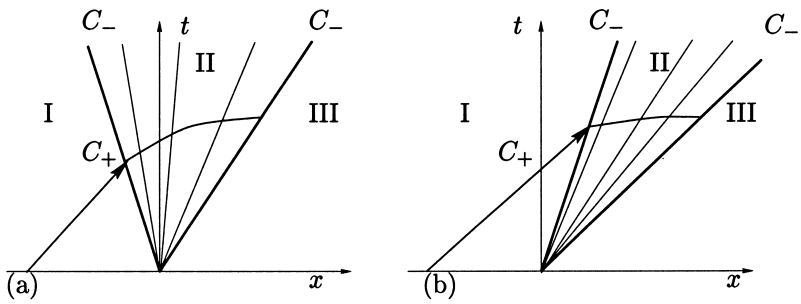

Figure 3. C_+ and C_- characteristic patterns used to solve the Riemann problem at the shoreline: (a) subcritical flow, (b) supercritical flow.

$$\frac{\mathrm{d}x}{\mathrm{d}t} = \lambda_{1_s} = u_s - c_s \quad (C_-) \tag{2.8}$$

see, for example, the detailed description in [9].

Finally, the (x, t)-plane is subdivided into three regions that characterize the solution of the shoreline Riemann problem: region II is made of an expansion fan of C_--type characteristics connecting conditions of regions I of left constant conditions $\mathbf{U}^{\mathrm{L}} = (d^{\mathrm{L}}, u^{\mathrm{L}}, d^{\mathrm{L}})$ with the dry conditions $\mathbf{U}^{\mathrm{R}} = (d^{\mathrm{R}}, u^{\mathrm{R}}, d^{\mathrm{R}}) = (0, 0)$ of region III.

Notice that along the C_- and C_+ characteristics Riemann variables $(\mathscr{R}_1, \mathscr{R}_2) = (u - 2c, u + 2c)$ are not conserved (as in the case of inviscid NSWEs) because of the presence of non-zero source terms which also include dispersive-non-linear contributions. On the contrary the following is valid:

$$\frac{\mathrm{d}\mathscr{R}_1}{\mathrm{d}t} = \mathscr{S} \quad \text{along } C_-, \qquad \frac{\mathrm{d}\mathscr{R}_2}{\mathrm{d}t} = \mathscr{S} \quad \text{along } C_+ \tag{2.9}$$

where $\mathscr{S} = S_2/d = gh_x - \tau_{\mathrm{b}} + D$.

It is, finally, essential to notice that SBCs are only a simplified version of

$$\frac{\mathrm{d}x_s}{\mathrm{d}t} = u_s \quad \text{or} \quad x_s = \int u_s \, \mathrm{d}t \tag{2.10a}$$

$$d_s = 0 \tag{2.10b}$$

and the purpose of any analyses dealing with SBCs is to suitably define u_s which appears in (2.10a) by obeying the constraint (2.10b).

Following Brocchini *et al.* [9] we compute u_s using conditions (2.9) in which $d_s = 0 \Rightarrow c_s = \sqrt{gd_s} = 0$ is used on the C_- characteristic which represents the shoreline

$$\frac{\mathrm{d}\mathscr{R}_1}{\mathrm{d}t} = \mathscr{S} \quad \text{along} \quad \frac{\mathrm{d}x_\mathrm{s}}{\mathrm{d}t} = u_\mathrm{s} \tag{2.11a}$$

$$\frac{\mathrm{d}\mathscr{R}_2}{\mathrm{d}t} = \mathscr{S} \quad \text{along} \quad \frac{\mathrm{d}x_\mathrm{s}}{\mathrm{d}t} = u^\mathrm{L} + c^\mathrm{L} \tag{2.11b}$$

Integration of these gives

$$\mathscr{R}_1(t+\Delta t) = \mathscr{R}_1(t) + \int_t^{t+\Delta t} \mathscr{S}\,\mathrm{d}t \quad \text{along} \quad \frac{\mathrm{d}x_\mathrm{s}}{\mathrm{d}t} = u_\mathrm{s} \tag{2.12a}$$

$$\mathscr{R}_2(t+\Delta t) = \mathscr{R}_2(t) + \int_t^{t+\Delta t} \mathscr{S}\,\mathrm{d}t \quad \text{along} \quad \frac{\mathrm{d}x_\mathrm{s}}{\mathrm{d}t} = u^\mathrm{L} + c^\mathrm{L} \tag{2.12b}$$

where in this case $[\mathscr{R}_1(t), \mathscr{R}_2(t)] = [u_\mathrm{s} - 2c_\mathrm{s}, u^\mathrm{L} + 2c^\mathrm{L}] = [u_\mathrm{s}, u^\mathrm{L} + 2c^\mathrm{L}]$.

Substitution into Equation (2.12) and knowledge of the integration path gives

$$\mathscr{R}_1(t+\Delta t) = u_\mathrm{s}(t) + \int_{x/u_\mathrm{s}}^{(x+\Delta x)/u_\mathrm{s}} \frac{\mathscr{S}}{u_\mathrm{s}}\,\mathrm{d}x \tag{2.13a}$$

$$\mathscr{R}_2(t+\Delta t) = u^\mathrm{L}(t) + 2c^\mathrm{L}(t) + \int_{x/(u^\mathrm{L}+c^\mathrm{L})}^{(x+\Delta x)/(u^\mathrm{L}+c^\mathrm{L})} \frac{\mathscr{S}}{u^\mathrm{L}+c^\mathrm{L}}\,\mathrm{d}x \tag{2.13b}$$

Notice that particular attention should be taken to evaluate integral contributions for small velocity values. At the shoreline this only occurs at the maximum run-up and run-down locations.

At the shoreline the above conditions are simultaneously valid (see Figure 3) hence giving the final result

$$u_\mathrm{s}(t) = u^\mathrm{L}(t) + 2c^\mathrm{L}(t) + \int_{x/(u^\mathrm{L}+c^\mathrm{L})}^{(x+\Delta x)/(u^\mathrm{L}+c^\mathrm{L})} \frac{\mathscr{S}}{u^\mathrm{L}+c^\mathrm{L}}\,\mathrm{d}x - \int_{x/u_\mathrm{s}}^{(x+\Delta x)/u_\mathrm{s}} \frac{\mathscr{S}}{u_\mathrm{s}}\,\mathrm{d}x \tag{2.14}$$

which replaces the condition

$$u_\mathrm{s}(t+\Delta t) = u^\mathrm{L}(t) + 2c^\mathrm{L}(t) \tag{2.15}$$

valid for NSWEs.

In the case of inviscid BTEs (i.e. with no seabed friction included) with purely dispersive extra contributions, $D \to 0$ in very shallow depths and the source term reduces to the acceleration due to the beach slope. Therefore (2.15) can suitably be used to evolve the shoreline position x_s in time through (2.10a) if either a splitting technique is used for such term Brocchini *et al.* [9] or the co-ordinate transformation by Watson *et al.* [12] is adopted. On the other hand, if D also contains non-linear-dispersive terms (a non-singular expansion in the non-linearity parameter must always be required) Equation (2.14) replaces (2.15).

3. THE SPECIFIC BTE

This section is dedicated to a brief description of the specific BTE model on which characteristic-type SBCs have been implemented. We have chosen to adopt and code this specific model described in length in [13,14], because of its effectiveness in representing near-shore flows.

3.1. The equations

The basic model equations are both the mass conservation equation

$$\zeta_t + [(h+\zeta)u_x] = 0 \tag{3.16}$$

and the momentum conservation equation

$$\begin{aligned} &u_t + uu_x + g\zeta_x + \left(B - \frac{1}{3}\right)h^2 u_{xxt} - \frac{1}{2}hh_{xx}u_t - hh_x u_{xt} + Bgh^2\zeta_{xxx} - \frac{1}{3}h^2 uu_{xxx} + \frac{1}{3}h^2 u_x u_{xx} \\ &- \frac{3}{2}hh_{xx}uu_x - \frac{1}{2}hh_{xxx}u^2 - hh_x uu_{xx} + Bh^2(uu_x)_{xx} - \frac{1}{3}h\zeta u_x u_{xx} \\ &- \frac{1}{3}hu_{xx}(\zeta u)_x + h(\zeta u_x^2)_x - \frac{2}{3}h(\zeta uu_{xx})_x - \zeta_x h_{xx}u^2 - \zeta h_x uu_{xx} - \frac{1}{2}\zeta h_{xxx}u^2 - \frac{3}{2}\zeta h_{xx}uu_x \\ &- \zeta_x h_x uu_x - \frac{1}{3}\zeta^2 uu_{xxx} - \zeta\zeta_x uu_{xx} + \zeta\zeta_x u_x^2 + \frac{1}{3}\zeta^2 u_x u_{xx} - h\zeta_x u_{tx} \\ &- \frac{2}{3}h\zeta(u_t)_{xx} + \zeta h_x(u_t)_x - h_x\zeta_x u_t - \frac{1}{2}\zeta h_{xx}u_t + \frac{1}{6}\zeta^2(u_t)_{xx} - \frac{1}{2}(\zeta^2(u_t)_x)_x = 0 \end{aligned} \tag{3.17}$$

with improved dispersion characteristics (here $B = -\frac{1}{15}$). Good dispersion properties, which make this model suitable for accurate flow predictions from the 'intermediate' to the 'shallow waters' have been obtained by retaining terms of order up to $O(\delta^3\mu^2)$ inclusive ($\mu = k_0 h_0$ and $\delta = a/h_0$ are the parameters which measure dispersion and non-linearity respectively and are built with $k_0 =$ characteristic wave number, $h_0 =$ characteristic depth and $a =$ characteristic wave amplitude).

Notice that, although the original form of Equation (3.17) includes additional terms which model energy dissipations caused by wave breaking, these are here neglected as our present purpose is to investigate shoaling and run-up of non-breaking waves. They will be re-introduced when modelling wave dynamics in the surf and swash zones. A second note of caution concerns the non-uniform validity of the expansion used to obtain (3.17). It is evident that the highest non-linear-dispersive terms of $O(\delta^3\mu^2)$, which are important to adequately model non-linearities in the outer and inner surf zone, are singular for $h \to 0$. Hence, they are not included in any analysis of swash motions.

3.2. The numerical model

The governing Equations (3.16) and (3.17) are solved using a numerical model based on a fourth-order Adam–Bashfort–Moulton (ABM) time-stepping scheme. This scheme, which is rather effective for BTEs [15], is also numerically efficient and easy to code. Suitable finite differences schemes are employed in order to obtain accurate estimates of spatial derivatives.

The independent variables x and t are discretized on the unstaggered grid by defining $x_i = (i-1)\Delta x$, $(i = 1, 2, \ldots, N_{\text{tot}} - 1, N_{\text{tot}})$ and $t_n = (n-1)\Delta t$, $(n = 1, 2, \ldots, T-1, T)$, where N_{tot} is the number of nodes of the computational domain in the x-direction and T is the number of time-steps. Since the numerical model should be able to simulate a moving shoreline, the computational domain is divided into two regions respectively a wet region (nodes from 1 to N) and a dry region (nodes from $N+1$ to N_{tot}) as depicted in Figure 4. The governing equations are solved only in the wet zone, and the abscissa x of the last wet node N represents the shoreline position. The value of N varies throughout the simulation depending on flow conditions as illustrated in detail in Section 4.

In order to apply the ABM scheme the governing equations are written in a more convenient way

$$\zeta_t = E \tag{3.18}$$

$$\tilde{u}_t = F \tag{3.19}$$

where

$$\tilde{u} = u + \left[\left(B - \frac{1}{3}\right)h^2 u_{xx} - \frac{1}{2}hh_{xx}u - hh_x u_x\right] \tag{3.20}$$

$$E = -[(h+\zeta)u]_x \tag{3.21}$$

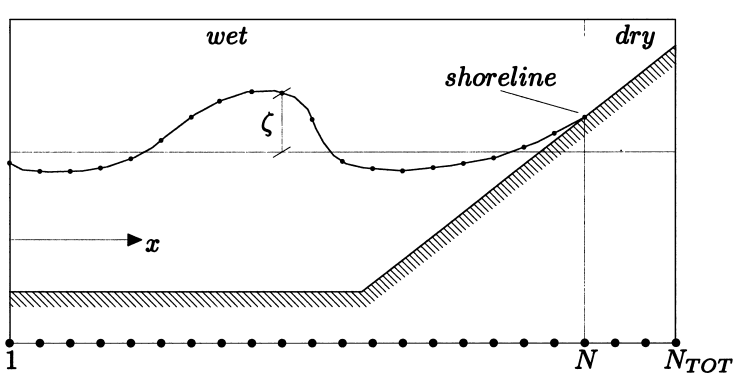

Figure 4. The computational domain.

and

$$F = -uu_x - g\zeta_x - Bgh^2\zeta_{xxx} + \frac{1}{3}h^2uu_{xxx} - \frac{1}{3}h^2u_xu_{xx} + \frac{3}{2}hh_{xx}uu_x + \frac{1}{2}hh_{xxx}u^2 + hh_xuu_{xx}$$
$$- Bh^2(uu_x)_{xx} + \frac{1}{3}h\zeta u_xu_{xx} + \frac{1}{3}hu_{xx}(\zeta u)_x - h(\zeta u_x^2)_x + \frac{2}{3}h(\zeta uu_{xx})_x + \zeta_xh_{xx}u^2 + \zeta h_xuu_{xx}$$
$$+ \frac{1}{2}\zeta h_{xxx}u^2 + \frac{3}{2}\zeta h_{xx}uu_x + \zeta_xh_xuu_x + \frac{1}{3}\zeta^2uu_{xxx} + \zeta\zeta_xuu_{xx} - \zeta\zeta_xu_x^2 - \frac{1}{3}\zeta^2u_xu_{xx} + h\zeta_xu_{tx}$$
$$+ \frac{2}{3}h\zeta(u_t)_{xx} - \zeta h_x(u_t)_x + h_x\zeta_xu_t + \frac{1}{2}\zeta h_{xx}u_t - \frac{1}{6}\zeta^2(u_t)_{xx} + \frac{1}{2}(\zeta^2(u_t)_x)_x \tag{3.22}$$

If initial conditions are specified, i.e. if the values of ζ and u at the time levels, n, $n-1$, $n-2$ are available, the solution at the subsequent time level $n+1$ can be obtained by means of the following procedure:

1. evaluation of right-hand sides of Equations (3.18) and (3.19) at time level n, $n-1$, $n-2$;
2. integration in time of Equations (3.18) and (3.19) by means of the predictor stage of the ABM scheme;
3. evaluation of u from $\tilde{u}$;
4. evaluation of right-hand sides of Equations (3.18) and (3.19) at time level $n+1$;
5. integration in time of Equations (3.18) and (3.19) by means of the corrector stage of the ABM scheme;
6. evaluation of u from $\tilde{u}$.

Steps 4–6 are iterated until convergence is reached.

In the following subsections the basic steps of the solution process are briefly described.

3.2.1. Evaluation of right-hand sides of Equations (3.18) and (3.19). The quantities E and F are function of ζ, u and of the spatial and time derivatives of such dependent variables.

For what concerns time derivatives, expressions consistent with the accuracy of the ABM scheme are adopted. As time derivatives depend on the future value of both ζ and u the value of F has to be computed anew at each iteration.

The spatial derivatives are computed by means of high-order finite difference scheme in order to obtain estimates with truncation errors lower than the highest-order dispersive terms in the governing equations. In the interior region of the domain central schemes can be applied while one-sided schemes are used to evaluate derivatives at the boundaries.

3.2.2. Integration in time of governing equations. Once right-hand sides of Equations (3.18) and (3.19) are computed estimates of quantities ζ and $\tilde{u}$ at the following time-step $n+1$ can be obtained by applying the ABM scheme which at the predictor stage reads

$$\zeta_i^{n+1} = \zeta_i^n + \frac{\Delta t}{12}[23E_i^n - 16E_i^{n-1} + 5E_i^{n-2}] \tag{3.23}$$

$$\tilde{u}_i^{n+1} = \tilde{u}_i^n + \frac{\Delta t}{12}[23F_i^n - 16F_i^{n-1} + 5F_i^{n-2}] \tag{3.24}$$

Once ζ_i^{n+1} and $\tilde{u}_i^{n+1}$ are estimated, the quantities E and F can be evaluated at the time-step $n+1$ and the corrector ABM expressions can be applied

$$\zeta_i^{n+1} = \zeta_i^n + \frac{\Delta t}{24}[9E_i^{n+1} + 19E_i^n - 5E_i^{n-1} + E_i^{n-2}] \tag{3.25}$$

$$\tilde{u}_i^{n+1} = \tilde{u}_i^n + \frac{\Delta t}{24}[9F_i^{n+1} + 19F_i^n - 5F_i^{n-1} + F_i^{n-2}] \tag{3.26}$$

The predictor–corrector scheme is applied to evaluate ζ_i^{n+1} for $i = 1, 2, \ldots, N-1, N$ and $\tilde{u}_i^{n+1}$ for $i = 2, 3, \ldots, N-2, N-1$, where N is, as stated before, the total number of wet nodes in the computational domain.

The depth-averaged velocity u can be obtained from $\tilde{u}$, when suitable boundary conditions are prescribed, solving a tridiagonal system by means of the technique described below.

3.3. Evaluation of u from ũ

Once the $\tilde{u}_i^{n+1}$ values are determined in all interior grid nodes ($i = 2, 3, \ldots, N-2, N-1$), a technique to solve the ordinary differential Equation (3.20) is needed to compute water velocity u. Equation (3.20) can be discretized using a three-point finite difference scheme for the second derivative of u and a simple two-point central finite difference scheme for the first derivatives to give

$$\tilde{u}_i^{n+1} = A_{i-1}u_{i-1}^{n+1} + B_i u_i^{n+1} + C_{i+1}u_{i+1}^{n+1} \quad \text{for} \quad i = 2, 3, \ldots, N-2, N-1 \tag{3.27}$$

These $N-2$ equations form a tridiagonal system that can be efficiently solved to obtain u_i^{n+1} at all interior grid points if u_1^{n+1} and u_N^{n+1} are specified.

It is stressed that the velocity at the boundaries at the time step u_1^{n+1} and u_N^{n+1} are requested by the numerical schemes as boundary conditions.

4. IMPLEMENTATION OF CHARACTERISTIC TYPE SBCS

In Section 2 the fluid velocity u_s^{n+1} at the interface between wet and dry states was obtained by solving the 'shoreline Riemann problem'. Now, in order to employ this solution as a boundary condition for the BTE model, some questions should be answered. First, where is the shoreline? Second, what is the difference (if any) between u_s^{n+1} and u_N^{n+1}? Third, how u_N^{n+1} can be evaluated from u_s^{n+1}?

Since the governing equations are discretized on a fixed spatial grid only an approximate answer can be given to the first question: the shoreline is somewhere between the last wet node N and the first dry node $N+1$. By changing the value of N, i.e. inundating and draining the nodes in the swash zone, shoreline movements can be tracked, but only a discrete

representation of the shoreline position can be obtained by the model at hand. In the following it is assumed that the shoreline is exactly in the middle of the region $[x_N, x_{N+1}]$, i.e. $x_s = x_N + \Delta x/2$. This assumption can easily be substituted by an interpolation procedure; which, however, would not alter the essence of the method. A technique to change the value of N when flow conditions require it is described in the following.

For what concerns the second question we can affirm that by assuming $u_N^{n+1} = u_s^{n+1}$ unrealistic and numerically unstable solutions are obtained by the BTE model. The reason is that u_s is the velocity of the fluid at a specific point (the shoreline) of the computational domain, while u_N^{n+1} should be representative of flow conditions in the region

$$\left[x_N - \frac{\Delta x}{2}, x_N + \frac{\Delta x}{2}\right]$$

A numerical technique to evaluate u_N^{n+1} from u_s^{n+1} is therefore needed. The basic assumption we start from is that u and ζ are piecewise constant over the three regions

$$\left[x_i - \frac{\Delta x}{2}, x_i + \frac{\Delta x}{2}\right]$$

$i = N-1,\ N,\ N+1$, hereinafter referred to as 'computational cells'. The quantities u_{N-1}^n, u_N^n and u_{N+1}^n can therefore be viewed as integral averages of the solution $u(x)^n$, namely

$$u_i^n = \frac{1}{\Delta x}\int_{x_{i-1/2}}^{x_{i+1/2}} u(x)^n \, \mathrm{d}x \tag{4.28}$$

Now a suitable numerical method is to be chosen in order to evaluate u_N^{n+1} starting from piece-wise constant initial conditions as depicted in Figure 6. It is necessary that the method can adequately deal with solution discontinuities (between cells $N-1$ and N) and treat the wet–dry interface between cells N and $N+1$ by taking the most from the accurate analysis performed in Section 2. Brocchini *et al.* [9] showed that a NSWE near-shore flow solver based on the weighted averaged flux (WAF) method can accurately simulate swash zone flows and shoreline motions. The WAF method is therefore adopted in the present study as the numerical tool to evaluate u_N^{n+1}, i.e. the boundary condition of the BTE model. It is stressed that this method is here merely used to convert the 'real' velocity value u_s into the 'numerical' value u_N^{n+1}.

4.1. A WAF technique to move the shoreline

The WAF method [16,17] is used to solve the conservative form of the NSWE. First, concentrate on the homogenous form of Equations (2.4), which is identical to the NSWE homogeneous problem for horizontal bottom.

$$\mathbf{U}_t + \mathbf{F}(\mathbf{U})_x = 0 \tag{4.29}$$

These equations can be integrated in a rectangular region of the $x-t$ space (see Figure 5) in order to obtain a weak form. Using Green's theorem

$$\oint [\mathbf{U}\,\mathrm{d}x - \mathbf{F}(\mathbf{U})\,\mathrm{d}t] = 0 \tag{4.30}$$

These equations can be solved on a staggered grid as depicted in Figure 5 if written in the following discrete form and for $i = N$

$$U_{k_N}^{n+1} = U_{k_N}^{n} + \frac{\Delta t}{\Delta x}\,[F_{k_{N-1/2}}^{n+1/2} - F_{k_{N+1/2}}^{n+1/2}], \quad k = 1, 2 \tag{4.31}$$

where $F_{k_{N-1/2}}^{n+1/2}$ and $F_{k_{N+1/2}}^{n+1/2}$ are the intercell fluxes at the time level $n+\frac{1}{2}$.

Several methods are available to estimate intercell fluxes $F_{k_{N-1/2}}^{n+1/2}$, $k = 1, 2$. Most of these solve the sub-grid initial value Riemann problem by means of exact or approximate techniques. Exact techniques provide an accurate solution of the initial value problem, but require more computational time than the approximate ones since an implicit equation is to be solved by iterations.

The Riemann problem at the interface between cells $N-1$ and N can be formulated as

$$\mathbf{U}_t + \mathbf{F}(\mathbf{U})_x = 0, \qquad \mathbf{U}(x, t_0) = \mathbf{U}_0(x) = \begin{cases} \mathbf{U}_{N-1} & \text{if } x < x_N - \Delta x/2 \\ \mathbf{U}_N & \text{if } x > x_N - \Delta x/2 \end{cases} \tag{4.32}$$

The structure of the solution in the $x-t$ plane is shown in Figure 6. It consists of two wave families, each of these emanating from the interface with propagation speed λ. The value of $\mathbf{U}^*$ in the region between the waves is computed here by means of an exact Riemann solver. Notice that the two wave families can be either rarefaction or shock waves, depending on the

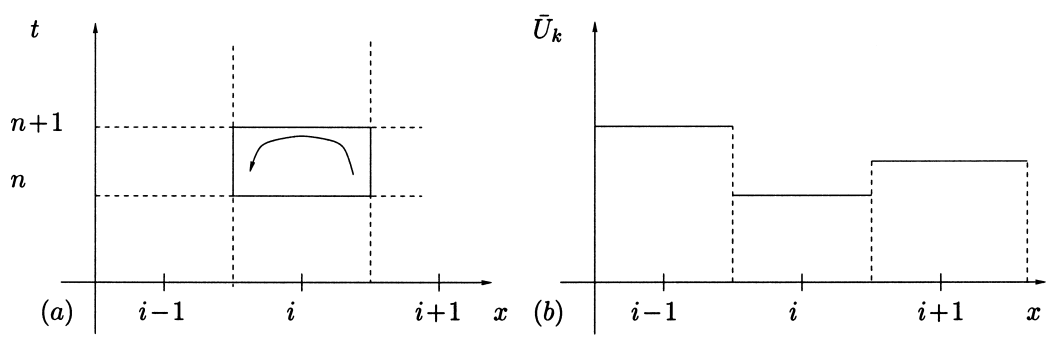

Figure 5. Variables representation on a discretized domain: (a) anticlockwise integration of (4.30) on a discretized $x-t$ space, (b) discrete solution behaviour.

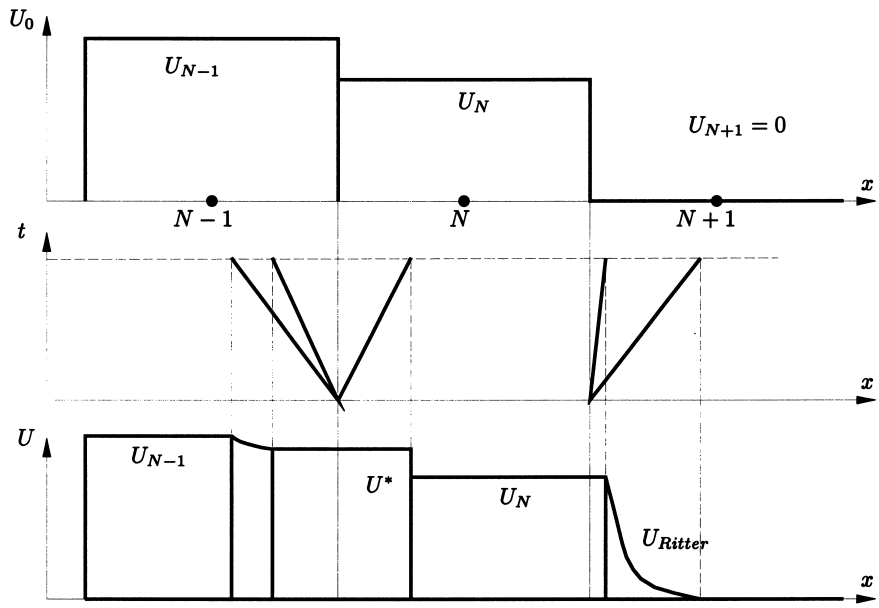

Figure 6. Example of solution of the 'shoreline Riemann problem' in the case of left rarefaction fan and a right shock wave.

initial values of the problem. In Figure 6 an example of a left rarefaction and a right shock is shown.

Once the Riemann problem is solved, fluxes in each region bounded by the waves can be computed. The value of the intermediate flux $F^{n+1/2}_{k_{N-1/2}}$, $k=1,2$ can be estimated by the weighted average of the fluxes over the region $[x_N, x_{N+1}]$ at the time level $n+1/2$.

At the interface between cells N and $N+1$ the Riemann problem reads

$$\mathbf{U}_t + \mathbf{F}(\mathbf{U})_x = 0, \qquad \mathbf{U}(x, t_0) = \mathbf{U}_0(x) = \begin{cases} \mathbf{U}_N & \text{if } x < x_N + \Delta x/2 \\ \mathbf{U}_{N+1} = 0 & \text{if } x > x_N + \Delta x/2 \end{cases} \tag{4.33}$$

The solution to this problem, already introduced in section 4, is known as Ritter's solution [11]; this consists of a rarefaction wave emanating from the interface (i.e. the shoreline at time level n) propagating with speed $(\lambda_1, \lambda_s) = (u_N - c_N, u_s)$, where λ_1 and λ_s are respectively the speed of the tail and head waves of the fan. In the region between the tail and the head of the rarefaction fan a quadratic dependence of the water depth on x and a linear dependence of the velocity on x is obtained by Ritter's solution. Particular care is required in evaluating the weighted averaged flux in this limit region. The final expression for $F^{n+1/2}_{k_{N+1/2}}$, $k=1,2$ adopted in the present study reads

$$F^{n+1/2}_{k_{N+1/2}} = \frac{1}{\Delta x}\left[\left(\lambda_1 \frac{\Delta t}{2} + \frac{\Delta x}{2}\right) F_k(d^{\mathrm{L}}, u^{\mathrm{L}}) + (\lambda_1 - \lambda_{\mathrm{s}}) \frac{\Delta t}{2} F_k(d^{\mathrm{L}}, u^{\mathrm{L}}, \tilde{d}, \tilde{u}, u_{\mathrm{s}})\right] \tag{4.34}$$

where $\tilde{d} = d^{\mathrm{L}}/2$, $\tilde{u} = (u^{\mathrm{L}} + u_{\mathrm{s}})/2$ and

$$F_k(d^{\mathrm{L}}, u^{\mathrm{L}}, \tilde{d}, \tilde{u}, u_{\mathrm{s}}) = \frac{1}{4} F_k(d^{\mathrm{L}}, u^{\mathrm{L}}) + \frac{1}{2} F_k(\tilde{d}, \tilde{u}) + \frac{1}{4} F_k(0, u_{\mathrm{s}}) \tag{4.35}$$

is the contribution from the region in the rarefaction fan computed by means of the trapezoidal rule.

u^{n+1}_N can be obtained by time-stepping the solution applying Equation (4.31) once intercell fluxes are computed. In order to solve Equations (2.4), which differ from (4.29) because of the presence of the source terms, we follow the approach of Watson *et al.* [12]. These authors proposed a technique based on the incorporation of the source terms into the Riemann problem. The idea is to transform the problem into a reference frame with horizontal acceleration equal to $g\alpha - D$, where α is the bottom slope assumed to be constant in each cell and D are the dispersive-non-linear terms. This transformation gives a set of homogenous equations that can be solved as described before. Then, by means of a reverse transformation, the solution is obtained in the original reference frame. Note, however, that D, unlike $g\alpha$, is not constant over each cell since its value depends on both the water depth and the velocity. To overcome this undetermination, D is assumed to be constant over Δt, given that this value is computed at the beginning of the time step.

The new variables in the accelerating reference frame are

$$\xi = x + \frac{1}{2}(g\alpha - D)t^2, \quad \tau = t$$

$$v = u + (g\alpha - D)t, \quad \chi = d \tag{4.36}$$

If these new variables are substituted into (2.4) a set of homogenous equations, formally identical to (4.29) is obtained. Once the solution is found in the accelerating frame, the reverse transformation yields the following relations between (4.36) and the original variables

$$u(x, t) = v\left[x + \frac{1}{2}(g\alpha - D)t^2, t\right] - (g\alpha - D)t$$

$$d(x, t) = \chi\left[x + \frac{1}{2}(g\alpha - D)t^2, t\right] \tag{4.37}$$

The structure of the solution of the Riemann problem in the case of a left rarefaction and a right shock wave is shown in Figure 7. The solution in the accelerating (panel a) reference frame is identical to the solution of Equations (4.29) while in the stationary frame (panel b) the trajectory of each wave is no longer a straight line but turns into a parabola.

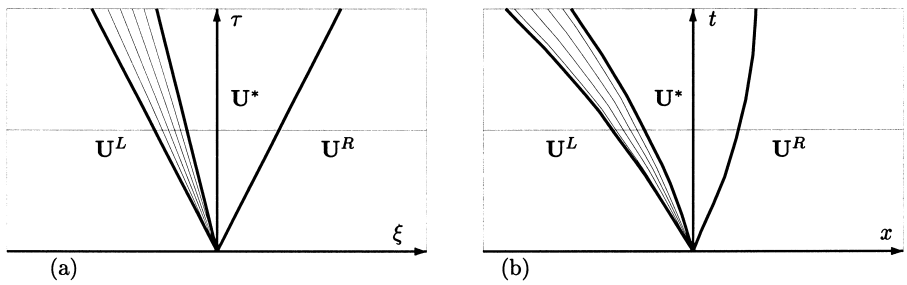

Figure 7. Riemann problem solution in the accelerating (a) and in the stationary (b) reference frames.

From a practical point of view, in order to apply the WAF method, the quantity $\frac{1}{2}(g\alpha - D)\Delta t$ must be subtracted from all the velocities and, in evaluating the weights of each flux, it is to be considered that the solution is shifted in x by a constant amount $\frac{1}{2}(g\alpha - D)(\frac{1}{2}\Delta t)^2$.

Equation (4.31), modified to take into account source terms effects reads

$$U_{k_N}^{n+1} = U_{k_N}^{n} + \frac{\Delta t}{\Delta x}\,[F_{k_{N-1/2}}^{n+1/2} - F_{k_{N+1/2}}^{n+1/2}] + S_N^{n+1/2}\Delta t, \quad k = 1, 2 \tag{4.38}$$

where

$$\mathbf{S}(\mathbf{U}) = \begin{bmatrix} 0 \\ -gd\alpha + dD \end{bmatrix} \tag{4.39}$$

[Notice that in the original work [12] because of a typographical error an incorrect expression for $\mathbf{S}(\mathbf{U})$ is reported on Equation (19).]

Finally, the technique to change the value of N during the run-up phase is based on the volume of fluid entering dry cell $N+1$ at each time step. An estimate of this volume can be obtained by applying the WAF method to the cell $N+1$. The expression (4.38) reads in this case

$$U_{k_{N+1}}^{n+1} = \frac{\Delta t}{\Delta x}\,[F_{k_{N+1/2}}^{n+1/2}] + S_{N+1}^{n+1/2}\Delta t, \quad k = 1, 2 \tag{4.40}$$

since $U_{k_{N+1}}^{n} = 0$, $k = 1, 2$ and $F_{k_{N+1/2}}^{n+1/2} = 0$, $k = 1, 2$.

If $d_{N+1}^{n+1}\Delta x$ is greater than a threshold value the cell is inundated and at the following time step the new value of $N = N + 1$ is employed.

During the run-down phase a simpler technique provides good results. This is based on the use of the water depth at node N: if d_N^{n+1} is lower than a threshold value at the following time step the new value of $N = N - 1$ is employed.

Note that in this work run-up and run-down phases were defined on the basis of flow direction at node $N-1$ at the time level n: $u^n_{N-1} > 0$ defines run-up, $u^n_{N-1} < 0$ run-down.

5. PERFORMANCE EVALUATION OF THE BTE MODEL WITH NEW SBCS

A number of tests are reported here to help the reader evaluate the performances of the implementation of the SBCs of Section 4 in the BTE model described in Section 3.

Analytical solutions are the most suitable for evaluating the performances of the implemented SBCs as they represent an exact benchmark. We consider here three important analytical solutions for waves propagating over a uniform sloping beach. They respectively model the run-up due to a depression of the water level (the fluid held motionless) which is suddenly released (the 'Carrier and Greenspan's run-up solution' [18]), the run-up and run-down characteristic of a periodic wave travelling shoreward and being reflected out to sea (the 'Carrier and Greenspan's standing wave solution' [18]) and the run-up of a solitary wave (the 'Synolakis run-up solution' [19]).

5.1. The Carrier and Greenspan run-up solution

This test corresponds to the physical in which the water level at the coastline of a plane uniform beach is depressed, the fluid held motionless and then released. It also represents the most classical test conditions for assessing the quality of any run-up solver.

Carrier and Greenspan [18] used a hodograph transformation to solve the NSWE and obtained an analytical solution of this problem. The transformation makes use of two dimensionless variables (hereinafter starred variables denote dimensionless quantities) (σ^*, λ^*) which are respectively a space-like and a time-like co-ordinate. Dimensionless ordinary variables and flow properties are then related to the hodograph co-ordinates as follows:

$$x^* = \frac{1}{4}\phi^*_\lambda - \frac{1}{16}\sigma^{*2} - \frac{1}{2}u^{*2}, \qquad t^* = \frac{1}{2}\lambda^* - u^* \tag{5.41a}$$

$$\eta^* = \frac{1}{4}\phi^*_\lambda - \frac{1}{2}u^{*2}, \qquad u^* = \phi^*_{\sigma^*}/\sigma^* \tag{5.41b}$$

where ϕ^* is a 'potential function' which depends on the specific propagation problem under investigation.

The 'run-up solution' is specified by the following initial conditions at $t^* = 0$:

$$\zeta^* = \epsilon\left[1 - \frac{5}{2}\frac{a^3}{(a^2+\sigma^{*2})^{3/2}} + \frac{3}{2}\frac{a^5}{(a^2+\sigma^{*2})^{5/2}}\right] \tag{5.42a}$$

$$u^* = 0 \tag{5.42b}$$

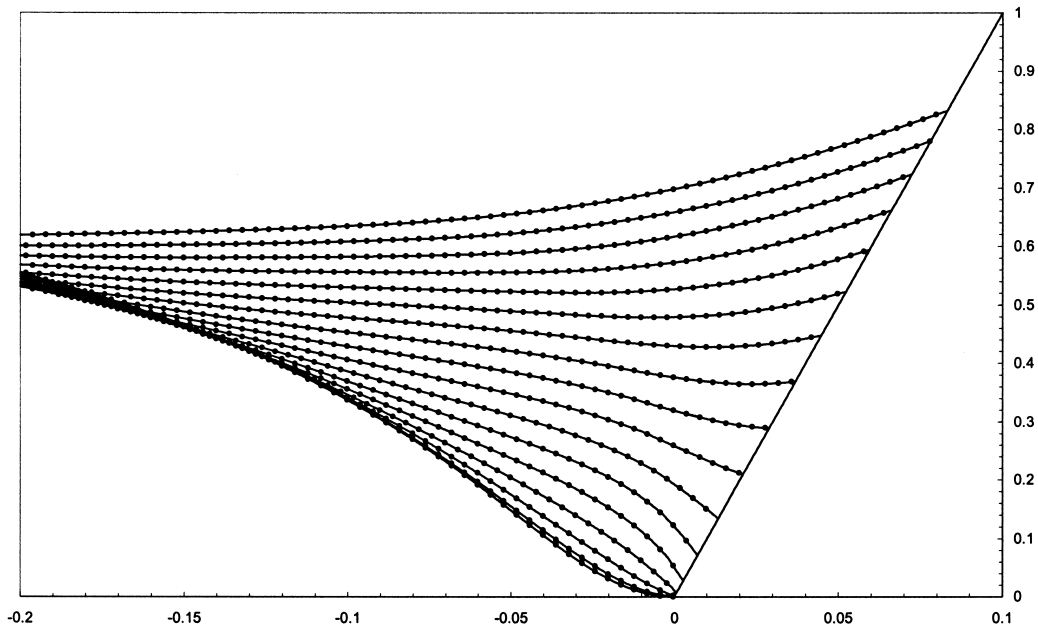

Figure 8. The 'Carrier and Greenspan run-up test' on a uniform plane beach. Dimensionless, scaled, analytical (dotted lines) and numerical (solid lines) profiles of water elevation ζ^* are plotted versus the dimensionless onshore co-ordinate x^* at dimensionless times increasing of $\Delta t^* = 0.05$ from $t^* = 0.00$ (bottom curves) to $t^* = 0.80$ (top curves).

$$x^* = -\frac{\sigma^*}{16} + \epsilon\left[1 - \frac{5}{2}\frac{a^3}{(a^2+\sigma^{*2})^{3/2}} + \frac{3}{2}\frac{a^5}{(a^2+\sigma^{*2})^{5/2}}\right] \tag{5.42c}$$

where $a = 3/2(1 + 0.9\epsilon)^{1/2}$ and ϵ is a non-linearity parameter.

Further details on both initial conditions and the analytical solution can be found in the original work of Carrier and Greenspan.

In Figure 8, which is the equivalent of figure 7 of [18], the analytical solution ζ^*/ϵ versus the onshore co-ordinate x^* is shown by means of dotted lines for different adimensional times. On the other hand, solid lines pertain to the numerical results while the thicker line represents the sloping seabed. It is evident that an excellent matching exists between the analytical and the numerical solution. It is also worth underlining that no spurious oscillations are present near the shoreline. Any oscillatory behaviours would reveal two possible sources of errors:

- a bad implementation of the SBCs in the chosen BTE model;
- a bad implementation of the 'wetting–drying' procedure.

On the contrary, the smooth behaviour of the elevation profiles of Figure 8 testifies to the absence of such problems.

5.2. The Carrier and Greenspan standing wave solution

This solution of the NSWEs represents the motion of a wave of dimensionless amplitude A^* and dimensionless frequency ω^* travelling shoreward and being reflected out to sea generating a standing wave [18]. In the past it has been widely used to analyse the dynamics of water waves approaching a coast or a continental shelf [20,21].

Such a solution can be specified by means of the following potential function

$$\phi^*(\sigma^*, \lambda^*) = A^* J_0(\omega^* \sigma^*) \cos(\omega^* \lambda^*) \tag{5.43}$$

where J_0 is the Bessel function of the first kind.

Once (5.43) is substituted into (5.41) a solution can be found for all the flow properties of interest in the ordinary (x^*, t^*)-space. Such a solution has been obtained both analytically and numerically for the case $A^* = 0.6$ $\omega = 1$ (non-breaking wave).

In Figure 9 both profiles of the numerically-computed free surface elevation and the envelope of the analytically-derived surface elevations are reported. The figure reveals an

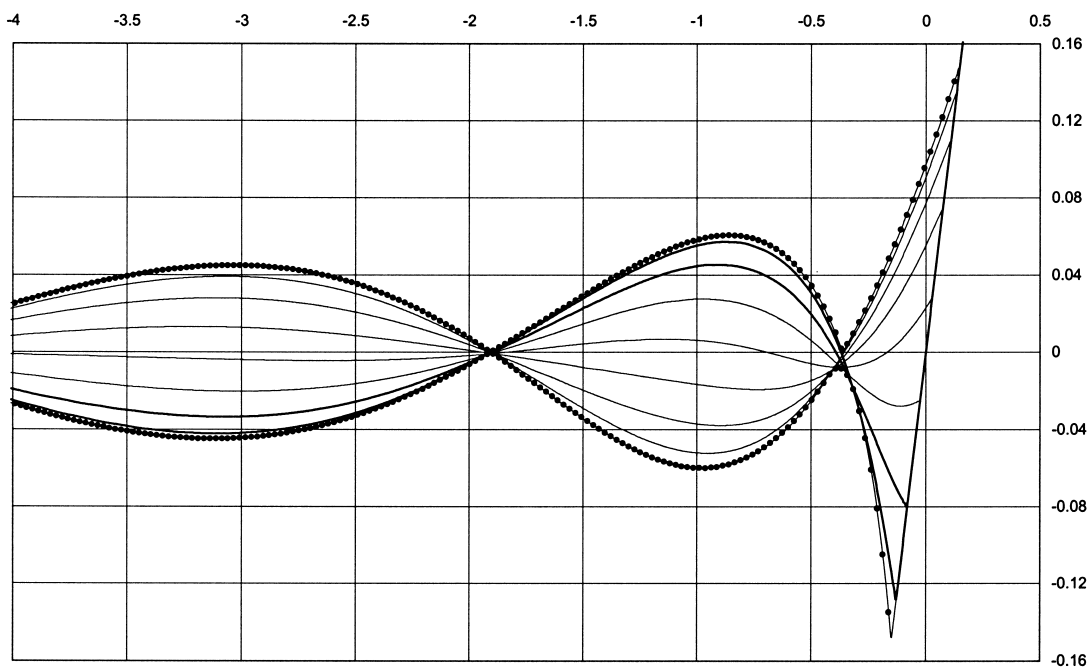

Figure 9. The 'Carrier and Greenspan standing wave test' on a uniform plane beach: envelope of surface elevations. Envelope of the dimensionless, analytical solution by Carrier and Greenspan (dotted lines) and numerical (solid lines) profiles of water elevation ζ^* are plotted versus the dimensionless onshore co-ordinate x^*.

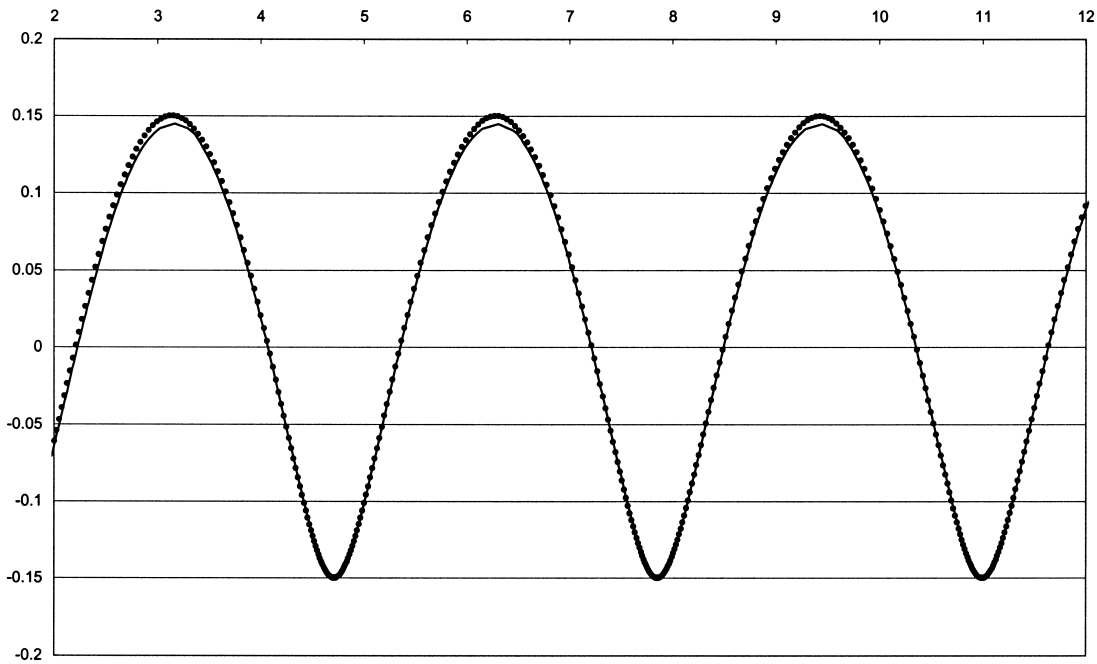

Figure 10. The 'Carrier and Greenspan standing wave test' on a uniform plane beach: horizontal motion of the shoreline. Incident wave of dimensionless amplitude $A^* = 0.6$ and dimensionless frequency $\omega^* = 1$. Dimensionless analytical shoreline path as from [18] (dotted line) and numerical shoreline path (solid line) in time.

almost perfect agreement between analytical and numerical solutions. Again, the absence of any oscillations in the numerical solution is particularly satisfying.

The comparison can also be pushed forward to analyse any possible differences in the horizontal motion of the shoreline. This is reported in Figure 10 in which a dotted line is used to represent the analytical solution while the solid line gives the numerical shoreline. Apart from a very small underestimation at the peak of the run-up (which could be fixed by increasing the spatial discretization) the numerical solution perfectly matches the analytical one. This does not happen when employing artificial techniques like the slot-technique [6], which always introduce a loss of mass (revealed by a reduced swash amplitude). The agreement is even more remarkable in view of the structure of the proposed SBCs which do not depend on any calibration parameters.

5.3. The Synolakis run-up solution

Synolakis' [19] solution is one of the very few available analytical solutions for the run-up of a solitary wave (a similar solution is also available for the interactions of solitary waves in

shallow waters [22]). Such an equation has been obtained in the framework of the NSWE but has been shown to model very well beach inundation conditions caused by solitary waves.

In Synolakis' solution a solitary wave of dimensionless height H^* centred at a distance X_1^* from the shore at time $t^* = 0$

$$\zeta^* = \frac{H^*}{d^*} \operatorname{sech}^2[\gamma(x^* - X_1^*)], \quad \text{where } \gamma = \sqrt{3H^*/4d^*} \tag{5.44}$$

is propagated over a combined topography made of a plateau of depth d^* and a plane sloping beach of slope β; matching of the two regions occurs at $x^* = X_0^* = \cot\beta$ (see Figure 11).

Propagation of the above signal by means of the NSWEs is more easily modelled if Carrier and Greenspan's [18] hodograph transformation and a Fourier transform technique are used in combination. This brings to the following definition for ϕ^*

$$\phi^*(\sigma^*, \lambda^*) = -\frac{32\mathrm{i}}{3} \int_{-\infty}^{\infty} \operatorname{cosech}(\xi k^*) \frac{J_0(k^*\sigma^* X_0^*/2)\, \mathrm{e}^{\mathrm{i}k^*\theta}}{J_0(2k^*X_0^*) - \mathrm{i}J_1(2k^*X_0^*)}\, \mathrm{d}k^* \tag{5.45}$$

where $\xi = \pi/2\gamma$ and $\theta = X_1^* - X_0^* + \lambda^* X_0^*/2$ is the pulse phase.

We refer the reader to [19] for a detailed description of the solution.

We used such a solution to illustrate the model performances to reproduce the run-up of a solitary wave. More specifically we have tried to reproduce Synolakis' results given in his figure 6. This summarizes the comparison of the analytical solution and experimental data in the case of solitary wave of $H^*/d^* = 0.019$ climbing up a 1:19.85 beach. Cross-shore profiles of the free surface elevation at different stages of the run-up process are reported in Figure 12. Notice that instead of centring the initial wave profile at $X_1^* = 37.35$ we used $X_1^* = 40$. This only introduces a small shift in the origin of the times.

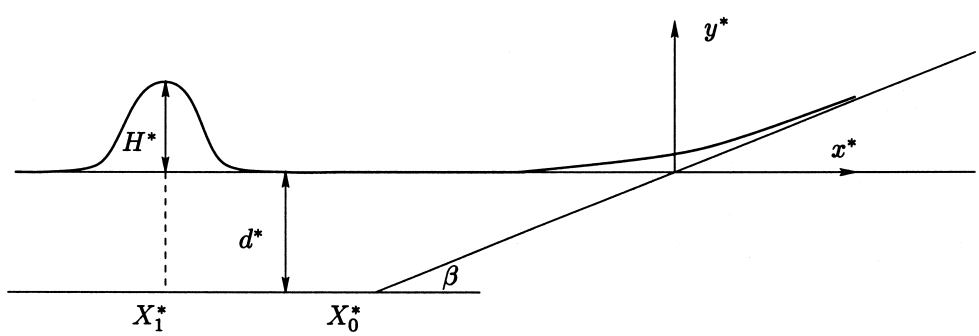

Figure 11. Definition sketch for the initial condition of Synolakis' run-up solution.

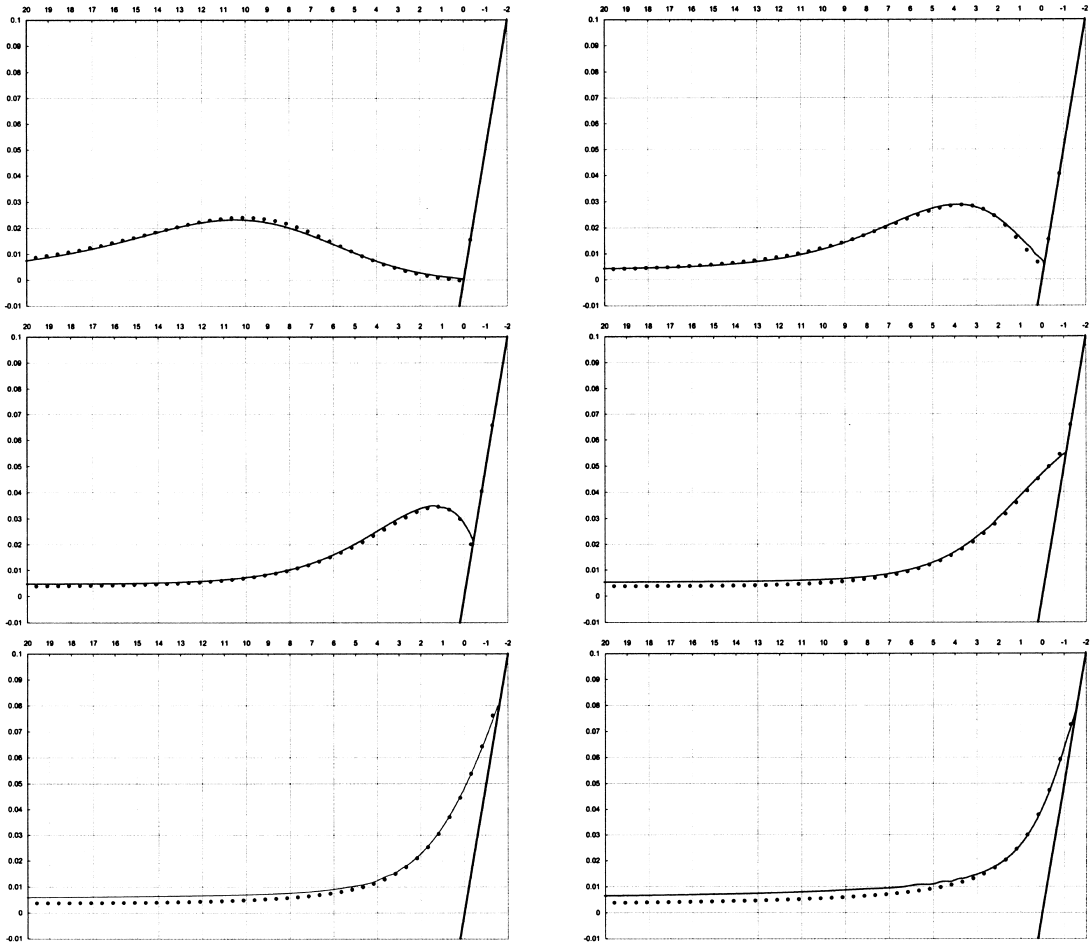

Figure 12. The 'Synolakis run-up solution'. Dimensionless free surface elevation ζ^* as function of the dimensionless x^* co-ordinate at different adimensional times $t^* = 20$, 30, 35, 40, 45, 50 (from left to right and from top to bottom). The solid line represents computed data while solid circles are used for Synolakis' analytical solution.

A very good matching exists between the numerical solution provided by the BTE model (solid lines) and Synolakis' analytical solution (dotted lines). The matching is almost perfect during most of the run-up. However, when the wave is just to reach the maximum run-up small discrepancies can be found far from the shore (i.e. $x^* > 10$). This discrepancy can be ascribed to the fact that being obtained within the NSWE framework Synolakis' solution best represents flow conditions near the shoreline.

However, near the shoreline (i.e. for $x^* < 4$) matching of the two solutions is always excellent, again suggesting a good implementation of the SBCs in the chosen BTE model.

6. CONCLUSIONS

A novel type of SBC has been proposed for Boussinesq-type models. This is derived by using the characteristic form of the NSWE and is shown to properly model the shoreline motion. The methodology used to implement such SBCs in a specific BTE model is illustrated and its effectiveness verified by means of three different analytical solutions. The illustrated model represents an efficient tool for modelling nearshore flows and analysis is underway to compare it with a shock-capturing version of the same BTE model in which non-linear-dispersive terms are regarded as forcings of the classical NSWEs.

ACKNOWLEDGMENTS

We thank Dr R. Bernetti for the many useful conversations and Professor P. De. Girolamo for carefully reading the manuscript. Support from the European Union through the contract EVK-2000-22038 is gratefully acknowledged.

REFERENCES

1. Peregrine DH. Long waves on a beach. *Journal of Fluid Mechanics* 1967; **27**: 815–827.
2. Brocchini M, Drago M, Iovenitti L. The modelling of short waves in shallow waters. Comparison of numerical models based on Boussinesq and Serre equations. *Proceedings of the 23rd International Conference on Coastal Engineering—ASCE* 1992; **1**: 76–88.
3. Schäffer HA, Madsen PA, Deigaard RA. A Boussinesq model for waves breaking in shallow waters. *Coastal Engineering* 1993; **20**: 185–202.
4. Madsen PA, Schäffer HA. Higher-order Boussinesq-type equations for surface gravity waves: derivation and analysis. *Proceedings of the Royal Society of London* 1998; **A356**: 3123–3184.
5. Brocchini M, Peregrine DH. Integral flow properties of the swash zone and averaging. *Journal of Fluid Mechanics* 1996; **317**: 241–273.
6. Madsen PA, Sørensen HA, Schäffer HA. Surf zone dynamics simulated by a Boussinesq-type model. Part I. Model description and cross-shore motion of regular waves. *Coastal Engineering* 1997; **32**: 255–287.
7. Özkan-Haller HT, Kirby JT. A Fourier–Chebyshev collocation method for the shallow water equations including shoreline runup. *Applied Ocean Research* 1997; **19**: 21–34.
8. Dodd N, Giarrusso C. ANEMONE: OTTO-1d, A user manual. HR Wallingford Report, 87, 2000.
9. Brocchini M, Bernetti R, Mancinelli A, Albertini G. An efficient solver for nearshore flows based on the WAF method. *Coastal Engineering* 2001; **43**: 105–129.
10. Bellotti G, Brocchini M. Wave shoaling and run-up by means of a Boussinesq-type model. *Atti del XXVII Convegno di Idraulica e Costruzioni Idrauliche* 2000; **IV**: 129–136.
11. Stoker JJ. *Water Waves*. Interscience: New York, 1957.
12. Watson G, Peregrine DH, Toro EF. Numerical solution of the shallow-water equations on a beach using the weighted average flux method. *Computational Fluid Dynamics* 1992; **1**: 495–502.
13. Veeramony J. Modelling the flow in surf zone waves. PhD dissertation, University of Delaware, 1999.
14. Veeramony J, Svendsen IA. The flow in surf zone waves. *Coastal Engineering* 2000; **39**: 93–122.
15. Wei G, Kirby JT, Grilli ST, Subramanya R. A fully nonlinear Boussinesq model for surface waves. I. Highly nonlinear, unsteady waves. *Journal of Fluid Mechanics* 1995; **294**: 71–92.
16. Toro EF. Riemann problems and the WAF method for solving twodimensional shallow water equations. *Philosophical Transactions of the Royal Society of London A* 1992; **338**: 43–68.
17. Toro EF. *Riemann Solvers and Numerical Methods for Fluid Dynamics*. Springer: Berlin, 1997.
18. Carrier GF, Greenspan HP. Water waves of finite amplitude on a sloping beach. *Journal of Fluid Mechanics* 1958; **4**: 97–109.
19. Synolakis CE. The run-up of solitary waves. *Journal of Fluid Mechanics* 1987; **185**: 523–555.
20. Carrier GF. Gravity waves on water of variable depth. *Journal of Fluid Mechanics* 1966; **24**: 641–659.
21. Carrier GF. Dynamics of tsunamis. In *Mathematical Problems in the Geophysical Sciences. Geophysical Fluid Dynamics*, vol. 1, Reid WH (ed.). American Mathematical Society, 1971.
22. Brocchini M. The run-up of weakly two-dimensional solitary pulses. *Nonlinear Proceedings in Geophysics* 1998; **5**: 27–38.

